doi:10.1016/j.jmb.2003.10.045 J. Mol. Biol. (2004) 335, 221–231

JMB

Available online at www.sciencedirect.com

SCIENCE DIRECT®

ELSEVIER

The Mechanism of Insulin Action on Islet Amyloid Polypeptide Fiber Formation

Jennifer L. Larson and Andrew D. Miranker*

Department of Molecular Biophysics and Biochemistry Yale University, 260 Whitney Avenue, New Haven, CT 06520-8114, USA

The pathology of type II diabetes includes the presence of cytotoxic amyloid deposits in the islets of Langerhans. The main component of these deposits, islet amyloid polypeptide (IAPP), is a hormone involved in glucose metabolism and is normally co-secreted with insulin by the β-cells of the pancreas. Here, we perform *in vitro* IAPP fibrillogenesis experiments in the presence and in the absence of insulin to elucidate the mechanism by which insulin acts on fiber formation. We find that insulin is an exceptionally potent inhibitor. In contrast to the vast excess of insulin over IAPP *in vivo*, substoichiometric amounts of insulin inhibit seeded and unseeded reactions by more than tenfold *in vitro*. Unusually, the magnitude of the inhibitory effect is dependent on the concentration of insulin, yet independent of the concentration of IAPP. In addition, insulin appears to bind non-specifically to fiber surfaces, giving rise to altered morphology. IAPP fiber formation *in vitro* requires a minimum of three steps: fiber-independent nucleation, elongation, and fiber-dependent nucleation. Furthermore, these steps are attenuated by the presence of a dispersed-phase transition. We interpret these data in the context of the phase-mediated fibrillogenesis model (PMF) and conclude through experiment and kinetic simulation that the dominant effect of insulin is to act on the elongation portion of the reaction. These results suggest that amyloid formation in type II diabetes involves either an additional agent that acts as an accelerant, or a step that segregates IAPP from insulin.

*Corresponding author

Keywords: IAPP; amylin; insulin; type II diabetes; amyloid

Introduction

The presence of amyloid deposits is a feature characteristic of a number of diseases including Alzheimer's, Parkinson's, and type II diabetes.[1,2] The predominant components of amyloid deposits are protein fibers, which are formed when a soluble amyloidogenic protein or peptide abnormally self-associates.[1] Although the sequence and native structure of amyloid precursor proteins vary from disease to disease, the resulting fibers share a number of structural characteristics. For example, visualization by electron microscopy reveals unbranched fibers with a diameter between 5 nm and 13 nm.[3] In addition, X-ray fiber diffraction studies indicate that the peptide backbone of all fibers adopts a cross β-structure.[3,4] In this structure, the individual β-strands are oriented perpendicular to the long axis of the fiber, while the hydrogen bonds are oriented parallel with the long axis of the fiber. Although the structures of amyloid fibers are similar, there is a high degree of specificity in amyloid formation. For example, studies on mammalian[5] and yeast[6] prion systems suggest that aggregates formed from identical protein sequences can have specific and propagatable conformations. Thus, while structural similarities suggest a common mechanism for fiber formation, specificity suggests that there exists a high degree of atomic order in these aggregated states.

Type II diabetes is a disease that afflicts more than 150 million individuals worldwide. The pathology of type II diabetes includes the presence of amyloid deposits in the islets of Langerhans in

Abbreviations used: IAPP, islet amyloid polypeptide; hIAPP, human IAPP; rIAPP, rat IAPP; HFIP, 1,1,1,3,3,3-hexafluoroisopropanol; NAYA, *N*-acetyl tyrosinamide; ThT, thioflavin T; PMF, phase-mediated fibrillogenesis model.

E-mail address of the corresponding author: andrew.miranker@yale.edu

over 90% of patients.[7–9] The main component of these deposits is islet amyloid polypeptide (IAPP), a 37 amino acid residue hormone that is stored with insulin in granules and secreted from the β-cells of the pancreas.[10,11] Although the exact role of amyloid in the pathogenesis of the disease is unclear, islet amyloidosis in patients with type II diabetes is associated with a reduced mass of insulin-producing β-cells.[7] In addition, IAPP fibers produced *in vitro* are cytotoxic to cultured β-cells.[12,13] Fiber formation is therefore an important factor in the development of β-cell failure. Little is known about the factors that lead to IAPP fiber formation *in vivo*. *In vitro*, wild-type and unmodified IAPP aggressively forms fibers at a concentration of 5 μM under near-physiological conditions.[14] This is far below the 800 μM concentration of IAPP present in secretory granules.[15] It is therefore more appropriate to question what prevents IAPP fiber formation in healthy people rather than what causes the phenomenon in diabetics.[16] Since IAPP isolated from amyloid fibers in diabetic patients is wild-type,[17] the obvious candidates for agents or conditions that might affect fiber formation are the other components of the granule. The key to such an investigation is an assessment of the kinetics of fiber formation in the presence and in the absence of components that are both known to be perturbed in diabetics, and known to perturb IAPP amyloid formation.

The kinetic profile of amyloid fiber formation is complex, as it occurs *via* a nucleation-dependent polymerization process not unlike crystallization.[18] This process is characterized by a slow, primary nucleation phase in which the protein forms an ordered nucleus, and a subsequent growth phase, which is dominated by elongation of the nucleus into larger fibers. One key feature of this type of polymerization is the ability to bypass the slow nucleation phase by the addition of preformed fibers, or "seed". Previously, we refined the nucleation-dependent polymerization model for IAPP to additionally include a secondary, or fiber-dependent, nucleation mechanism and phase partitioning elements. These steps were required in order to describe the kinetics observed *in vitro*.[14] This model, termed dispersed, phase-mediated fibrillogenesis (PMF), describes explicit events on the fiber formation pathway and serves as a framework for testing the effects of insulin on IAPP fiber formation.

IAPP and insulin are genetically and biochemically related. They possess common promoter sequences, are synthesized as pro-peptides in the β-cell, and are proteolytically processed by the same pro-hormone convertases.[7] Inhibition of IAPP fiber formation by insulin was first demonstrated using a histological stain, Congo red.[16] This contrasts with earlier studies in which radiolabeled IAPP associated with unlabeled fibers more readily when insulin was present.[19] More recent studies, however, confirm that insulin possesses an ability to inhibit IAPP fiber formation. These include solution-based assays, which used insulin at concentrations at or in excess of the concentration of IAPP to show inhibition.[20,21] As there are several steps in the IAPP fiber formation reaction (see above), an understanding of the mechanism requires that we identify the target of the inhibitory action of insulin. Our approach in this work is to use fluorescence, mass spectrometry, and electron microscopy to make detailed measurements of IAPP fibrillogenesis. Fiber formation reactions are performed in the presence and in the absence of insulin, and in the presence and in the absence of IAPP seed. As our measurements are in real time and have high signal to noise ratios, we are able to distinguish possible mechanisms by which insulin alters fiber formation in the context of the PMF model.

Results

Fiber assembly by IAPP involves a minimum of four processes: primary nucleation, elongation, secondary nucleation, and phase partitioning. Primary nucleation is the process by which IAPP associates to form a stable nucleus. Elongation is the process by which the nucleus grows to form long fibers. Secondary nucleation is any nucleation process by which new fibers are made at a rate that is dependent on the amount of fiber already present. Lastly, phase partitioning of IAPP attenuates the apparent concentration-dependence of the three other processes. In order to delineate the effect of insulin on these separate events, we examine the effect of insulin on *de novo* fibrillogenesis reactions and on reactions in which the lag phase of fiber formation is bypassed by addition of preformed seed. Attenuation of amyloid formation kinetics by insulin can be expected to alter the morphology of resulting fibers in a manner indicative of the underlying mechanism. We therefore use transmission electron microscopy to visualize this change, and mass spectrometry to assess association of insulin with IAPP fibers quantitatively.

De novo fiber formation

IAPP fiber formation is readily inhibited by substoichiometric quantities of insulin. Fiber formation reactions are initiated by dilution of a stock solution of IAPP in hexafluoroisopropanol (HFIP) into reaction buffer (pH 7.4, 25 °C, ionic strength isotonic with serum). Fiber formation by IAPP is then measured in real time by fluorescence anisotropy (Figure 1(a)). This method capitalizes on the fact that IAPP possesses a single intrinsic tyrosine residue that has two distinct anisotropic values, reflecting unstructured precursor and rigid fibrillar conformations.[22] As IAPP is consumed completely in these reactions (see below), reaction kinetics in this work are normalized on the *y*-axis to represent the fraction of monomeric IAPP

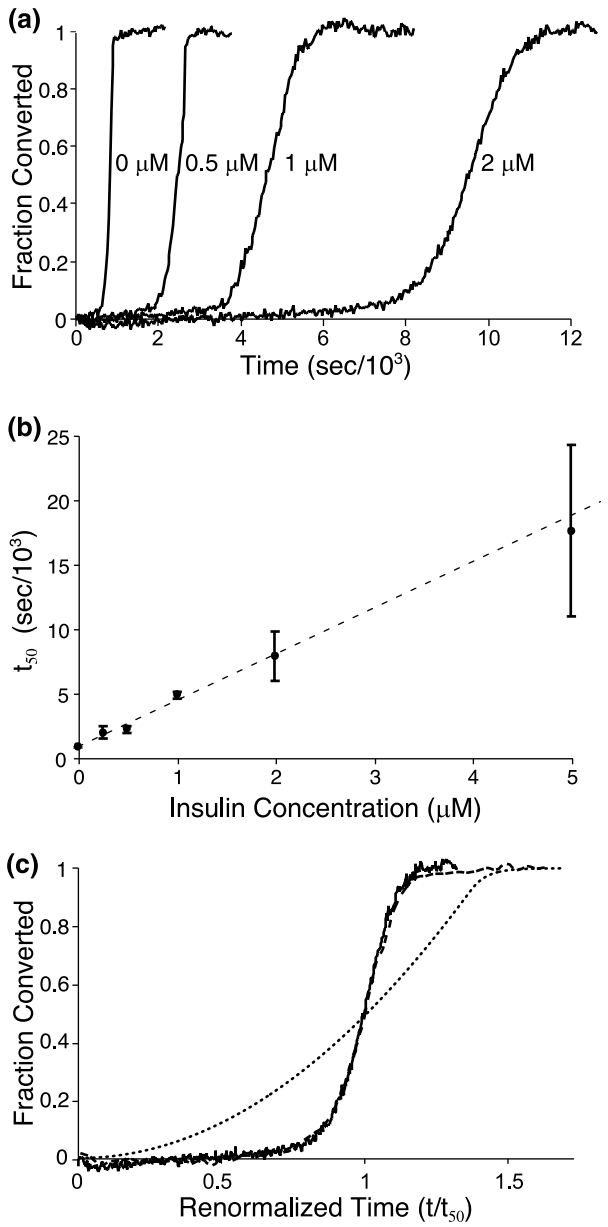

Figure 1. The effects of insulin on IAPP fibrillogenesis. IAPP fiber formation is monitored by changes in fluorescence anisotropy. Kinetic profiles are renormalized to show the fraction of IAPP converted to fiber form. (a) Representative kinetic profiles are shown with initial concentration of 25 μM IAPP and various concentrations of insulin. (b) Time for 50% conversion (t_{50}) is calculated at each concentration of insulin, performed in triplicate. A straight broken line is drawn as a guide. (c) A time axis-renormalized plot for a representative 25 μM IAPP reaction with 2 μM insulin (continuous line), and an otherwise identical reaction without insulin (broken line). For comparison, a simulated reaction (see Materials and Methods) in which secondary nucleation is eliminated is overlaid (dotted line).

converted into fiber form. This renormalization serves to remove any differences in fluorescence anisotropy that may arise from the presence of insulin in the reaction. Under the conditions used here, 25 μM IAPP reactions in the absence of added insulin display complete conversion within ~1000 seconds (Figure 1(a)). Addition of as little as 2 μM insulin to a 25 μM IAPP reaction increases the time for conversion eightfold (Figure 1(a)). Insulin is clearly able to inhibit fiber formation at concentrations well below those of IAPP. In these kinetics, a standard parameter is considered, t_{50}, defined as the time at which one-half of the material has converted to fiber form. As the concentration of insulin in the IAPP fiber formation reaction increases, the t_{50} increases linearly in a dose-dependent manner (Figure 1(b)).

Kinetics of IAPP fiber formation in the presence of substoichiometric quantities of insulin display the same degree of secondary nucleation as those formed without insulin. Kinetic profiles that differ in polymerization mechanism, i.e. single *versus* double nucleation mechanisms, can be distinguished readily on a time axis-renormalized plot.[23] Renormalization is performed by expressing the time axis as (actual time)/t_{50}. To determine whether fiber formation inhibition by addition of insulin differs in profile from reactions performed in the absence of insulin, we compare the renormalized kinetics of a 25 μM IAPP reaction in the presence and in the absence of 2 μM insulin. These reactions differ in t_{50} by nearly a factor of 10, but overlay almost exactly on a renormalized plot (Figure 1(c)). For comparison, a simulation of a reaction in which no secondary nucleation is present is overlaid. As the experimental reactions display no change in renormalized profile, this suggests that there has been no significant change in relative levels of primary *versus* secondary nucleation mechanisms.

The magnitude of the effect of insulin on IAPP fiber formation is insensitive to the concentration of IAPP. We previously reported that under our conditions, the kinetics of IAPP fiber formation are insensitive to IAPP concentration.[14] It is mechanistically informative to determine if this holds true when fibers are formed in the presence of insulin. We monitored the kinetics of 25 μM and 10 μM IAPP reactions each in the presence and in the absence of 2 μM insulin (Figure 2(a)). In the absence of insulin, t_{50} is 580(±120) seconds and 810(±40) seconds for 10 μM and 25 μM reactions, respectively, consistent with our previous report of concentration-independence. In the presence of 2 μM insulin, t_{50} is 8100(±830) seconds and 7900(±1900) seconds, respectively (Figure 2(b)). The t_{50} values of these reactions are within experimental error, demonstrating that insulin acts on concentration-independent elements of the fiber formation reaction.

Seeded kinetics

In order to delineate the effect of insulin on fiber formation in the absence of primary nucleation, we determined the effect of insulin on seeded fiber formation reactions. The kinetics of seeded IAPP

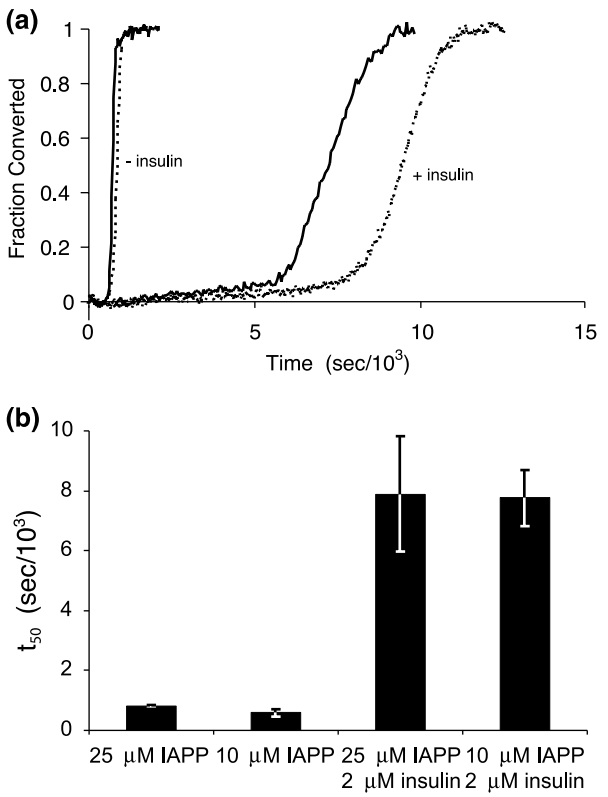

Figure 2. The effect of a fixed concentration of insulin on fibrillogenesis with various concentrations of IAPP. Fibrillogenesis reactions of (a) 25 μM (continuous line) and 10 μM (dotted line) IAPP were prepared either alone, or with 2 μM insulin. Representative curves for each solution are shown. (b) Time for 50% conversion (t_{50}) for at least three reactions is calculated for each solution.

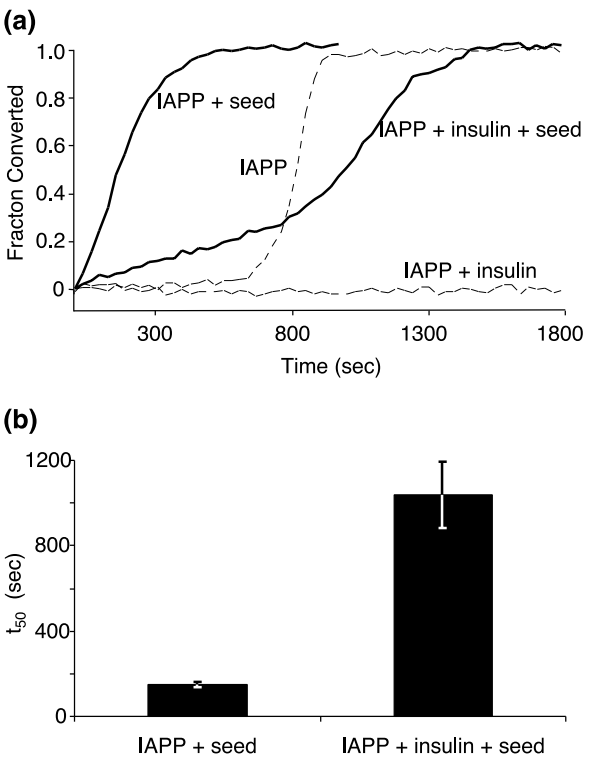

Figure 3. Insulin inhibits seeded IAPP reactions. (a) Representative fiber formation reactions containing 25 μM IAPP and 2 μM fiber seed (in monomer units) were prepared with and without 2 μM insulin (continuous lines). Corresponding reactions containing no fiber seed are shown truncated at 1800 s (broken lines). (b) Times for 50% conversion (t_{50}) for at least three seeded reactions were calculated.

reactions is inhibited by the presence of insulin (Figure 3). We have demonstrated that substoichiometric seeding of IAPP reactions bypasses the lag phase of the *de novo* counterpart completely.[14] For example, a *de novo* 25 μM IAPP reaction reaches 10% conversion in ~700 s (Figure 3(a)). By contrast, seeding with 2 μM preformed fibers (in monomer units) gives a reaction that is 90% complete in ~300 seconds. The complete bypass of the lag phase with preformed seed can similarly be seen in reactions containing 2 μM insulin (Figure 3(a)). This indicates that primary nucleation makes little, if any, contribution to the seeded kinetics. For the 25 μM IAPP reaction containing 2 μM seed, we measure a t_{50} of 150(±10) seconds (Figure 3(b)). The same reaction performed in the presence of 2 μM insulin gives a t_{50} of 1000(±150) seconds. Thus, IAPP seed has accelerated the insulin inhibited reaction by about eightfold which is comparable to the approximately fivefold acceleration observed for seeding of the same reaction in the absence of insulin. If the dominant effect of insulin was to slow primary nucleation, addition of seed would have negated the inhibitory action of insulin.

Ultrastructural analysis

Higher-order IAPP fiber aggregation is perturbed by formation in the presence of insulin. Fiber solutions were produced from 25 μM IAPP reactions performed alone, or in the presence of 2 μM or 5 μM insulin. These were negatively stained and analyzed by electron microscopy (Figure 4). Subjective bias was eliminated by withholding sample identities until after image collection and analysis were complete. Transmission electron microscopy (TEM) images in the presence and in the absence of insulin showed small clumps of straight fibers approximately 10 nm in width, and between 200 nm and 400 nm in length (Figure 4(a),(c) and (d)). This is consistent with previously reported TEM and atomic force microscopy (AFM) observations.[24,25] However, fibers formed in the absence of insulin contain many mat-like assemblies of fibers that are several micrometers in size (Figure 4(b)). Fiber mats were not observed in reactions of IAPP performed in the presence of either 2 μM or 5 μM insulin. This suggests that insulin affects higher-order assembly of IAPP after fiber formation is complete.

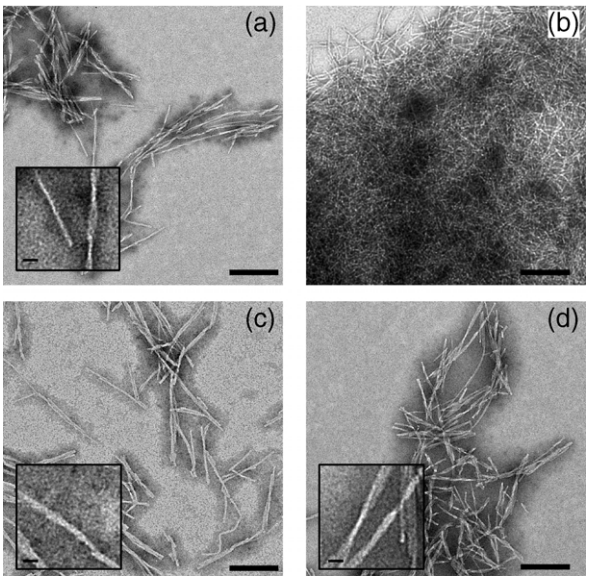

Figure 4. Electron microscopy of IAPP fibers formed with and without the presence of insulin. Negative stain transmission electron micrograph of IAPP fibers generated with (a) and (b) 25 μM IAPP, (c) 25 μM IAPP with 2 μM insulin, or (d) 25 μM IAPP with 5 μM insulin. The scale bars represent 200 nm in full images and 20 nm in insets. Under all conditions, IAPP forms fibers that are, on average, 10 nm in width and between 200 nm and 400 nm in length. Only the sample of IAPP fibers produced in the absence of insulin displayed large mats of aggregated fibers (b). Samples were coded to blind the operator (J.L.) before observation and analysis.

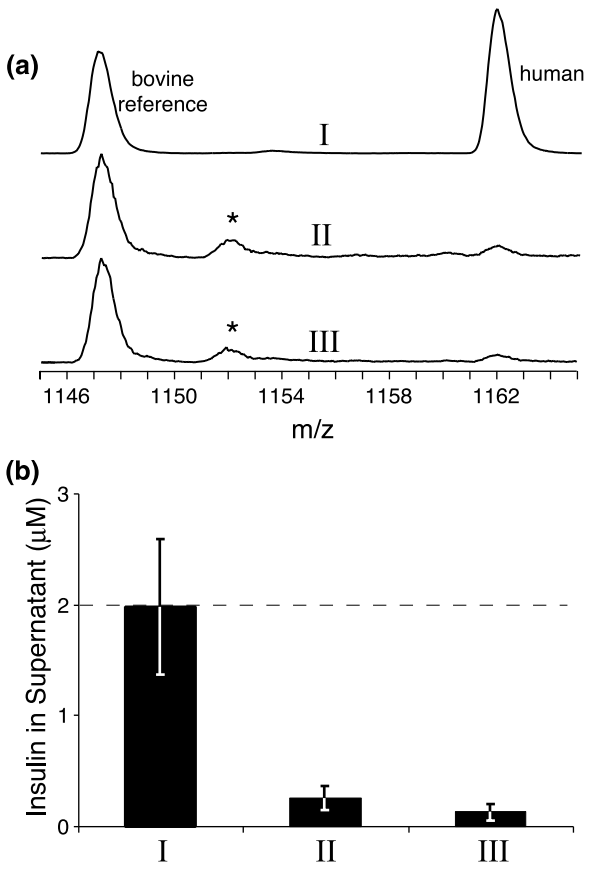

Figure 5. Mass spectrometry analysis of soluble protein concentration. (a) Electron spray ionization mass spectrometry (ESI-MS) spectra of soluble insulin. Insulin (2 μM) was incubated alone (I), added to unpolymerized 25 μM IAPP (II), or added to 25 μM IAPP (in monomer units) fibers (III). Samples were incubated for three hours to allow IAPP fiber formation to occur in the unpolymerized sample. The solution was then spun at 18,000*g* to remove fibers and analyzed by ESI-MS for soluble insulin using a 2 μM bovine insulin standard. (b) Human insulin peaks in (a) were integrated and compared to the standard to quantify the amount of unbound insulin. (Starred peaks denote a Na^+ adduct of the bovine insulin standard.)

Insulin binding to IAPP fibers

Inhibition of IAPP fiber formation and higher-order fiber aggregation may be mediated by insulin binding to IAPP fibers. To further investigate the interaction between IAPP fibers and insulin, we sought to determine if insulin could be incorporated into IAPP fibers. To address this, a 25 μM IAPP fiber formation reaction containing 2 μM insulin was prepared. After completion of the reaction, solutions were centrifuged to remove fibers and the concentration of insulin in the supernatant was analyzed by mass spectrometry (Figure 5(a)). Mass spectrometry can be used to determine the concentration of an individual protein in a mixture by introduction of a closely related internal standard.[26] Our standard in this case is bovine insulin, which differs in mass from human insulin by 74 Da. Figure 5(b) shows that the amount of insulin that remained in the supernatant is 0.3(±0.1) μM. This indicates that most of the insulin has associated with IAPP fibers during the course of the reaction. To determine whether insulin was actually incorporated into fibers during the polymerization reaction or simply associated with IAPP fibers, we added 2 μM insulin to 25 μM (in monomer units) of preformed IAPP fibers. The results indicate that 0.1(±0.1) μM insulin remains in the supernatant. Thus, nearly all of the insulin has associated with the preformed fiber solution. Therefore, although we cannot rule out the possibility that insulin is being incorporated into IAPP fibers during the reaction, the extent of insulin association with IAPP can be accounted for completely by insulin binding to fiber already formed.

Extent of reaction

It is possible that the target of insulin is disruption of the fiber formation equilibrium in a manner such that more soluble IAPP exists at the end of the reaction. Addition of insulin does not, however,

affect the degree of completion of IAPP fiber formation. Reactions containing 25 μM IAPP, ±2 μM insulin were prepared. After completion of fiber formation, solutions were centrifuged as above, and rat IAPP was doped into the supernatants to act as an internal standard for mass spectrometry. We did not observe any soluble IAPP at the end of IAPP fiber formation reactions performed with or without insulin (data not shown). Therefore, insulin does not appear to alter the concentration of IAPP in the fiber state significantly. Alternatively, insulin may be promoting the formation of amorphous IAPP aggregates. Our mass spectrometric method cannot make this distinction. This possibility is unlikely, however, since TEM analysis (Figure 4(c) and (d)) of the insulin-containing reactions shows no amorphous aggregates.

Discussion

Determining the effect of insulin on the kinetics of IAPP fiber formation is necessary to fully understand the progression of type II diabetes. Here, we perform *in vitro* IAPP fibrillogenesis experiments in the presence and in the absence of insulin. We observe several behaviors of insulin action. (i) Insulin acts at substoichiometric concentrations to slow overall (i.e. t_{50}) IAPP fiber formation. (ii) The inhibitory effect of insulin on fiber formation is independent of the starting concentration of IAPP. (iii) Insulin slows the overall conversion times of seeded IAPP fiber formation reactions. (iv) Insulin does not affect the extent of IAPP conversion into fibers. (v) Fibers formed in the presence of insulin display less high-order aggregation. (vi) Insulin associates with IAPP fibers whether it is present during the fiber formation reaction or added after fibrillogenesis is complete.

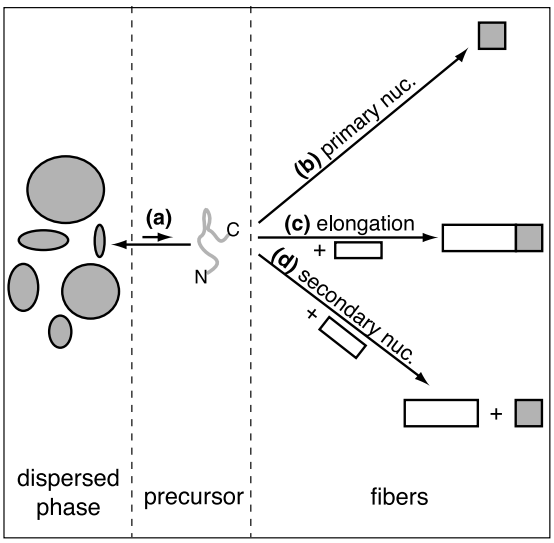

Figure 6. A schematic of the phase-mediated fibrillogenesis (PMF) model[14] with possible sites of insulin inhibition: (a) dispersed/aqueous phase equilibrium; (b) primary nucleation; (c) elongation; (d) secondary nucleation.

We interpret the results of our study of insulin inhibition of IAPP fiber formation in the context of the PMF model that has been described by members of our laboratory (Figure 6).[14] According to the PMF model, the aqueous concentration of IAPP monomer during the reaction is kept constant by the presence of a dispersed phase (Figure 6(a)). Aqueous IAPP then undergoes a slow association to form primary nuclei (new fiber ends) (Figure 6(b)). IAPP monomer can associate with these primary nuclei during the elongation process (Figure 6(c)). As the reaction proceeds, the amount of fiber in the reaction increases and secondary nucleation begins to occur as a second-order process, dependent on both aqueous IAPP concentration and the amount of fiber already formed (Figure 6(d)).

The possibility that insulin acts directly on the dispersed phase can be excluded (Figure 6(a)). Interactions between insulin and the dispersion could result in changes in the stability of the dispersion or the dissolution rate of IAPP from the dispersed to aqueous phases. For instance, if the dispersion is rendered more stable, the effective concentration of soluble IAPP would be diminished, and therefore the nucleation time could reasonably be expected to become slower. It is a property of dispersions that they have a characteristic size distribution. This results in the total volume and surface area varying linearly with total IAPP. The consequence of this on possible mechanisms is that the inhibitory effect of insulin should be dependent on the mole ratio of insulin:IAPP. As the inhibition of IAPP fiber formation by insulin is independent of the concentration of IAPP (Figure 2), it is unlikely that the dispersed phase has been affected directly.

Insulin does not interact directly with soluble IAPP to inhibit primary nucleation (Figure 6(b)). A consequence of the PMF model is that, above a critical concentration, the dispersed phase provides a constant concentration of soluble IAPP for reaction initiation. Under the conditions used here, the critical concentration is less than 5 μM.[14] Kinetics in this work are delayed appreciably even at small ratios of insulin to IAPP (Figure 1). Over any modest range of insulin:IAPP binding stoichiometries, these low concentrations of insulin would merely extract some of the soluble IAPP from the pool participating in primary nucleation. As the dispersed phase would replenish the soluble IAPP lost, the kinetics should not be changed. In addition, if insulin were able to inhibit only primary nucleation, it would have no effect on reactions where primary nucleation has been bypassed by seeding. Clearly, this is not the case, as the kinetics of seeded IAPP reactions are greatly diminished in the presence of

insulin (Figure 3). Consequently, primary nucleation can be eliminated as a target of insulin inhibition.

Insulin does not appear to inhibit fiber-dependent nucleation processes (Figure 6(d)). One mechanism of secondary nucleation is that new fibers may be created by nucleating off of the non-growing surface of the fiber. In the context of this possibility, our observation that insulin binds to fibers (Figure 5(a) and (b)), could give rise to inhibition of secondary nucleation. However, our kinetic analysis suggests otherwise. Fibrillogenesis reactions that include secondary nucleation processes can be distinguished readily from those that display only a single nucleation process on a time axis-renormalized plot (Figure 1(c)).[23] Secondary nucleation processes give rise to new fiber ends in a manner that accelerates as the reaction proceeds towards completion. On a time-renormalized plot, this gives rise to the appearance (short transitions and flat lag-phase) of cooperativity. The kinetics of IAPP fibrillogenesis in the absence of insulin display a sharp cooperative transition that cannot be accounted for without fiber-dependent nucleation processes.[14] The addition of 2 μM insulin increases the time for completion of the reaction by approximately eightfold. If the principal action of insulin were to inhibit secondary nucleation, we would expect that the time-renormalized plot of an insulin-inhibited reaction would shift in profile to more resemble that of primary nucleation only. In fact, the profile of the insulin-inhibited reaction is identical with the same reaction performed without insulin.

A second manifestation of secondary nucleation processes is the presence of an inflection point in the profile of seeded kinetics. Seeded reactions containing 25 μM IAPP, 2 μM insulin and 2 μM seed (in monomer units) are complete within ~1500 seconds (Figure 3). This is within the lag phase of the corresponding unseeded reaction, ~6000 seconds. We have therefore bypassed primary nucleation completely in the seeded reactions containing insulin. If the seeded reaction were deficient in secondary nucleation in the presence of insulin, fiber formation would simply result in the elongation of the added pool of fiber ends. In such a case, only exponential kinetics would be visible. However, the seeded kinetics is clearly more complex in the presence of insulin, as we see a profile with an inflection point. This indicates that there are at least two processes occurring in the seeded reaction: elongation and secondary nucleation. Combined with our observations on *de novo* kinetics, we assert that insulin does not act directly on secondary nucleation processes.

The elimination of dispersed/aqueous phase equilibrium, primary nucleation, and secondary nucleation as candidate targets for insulin inhibition enables us to assert that insulin is acting on the elongation portion of the IAPP reaction (Figure 6(c)). To test the plausibility of this, we have extended our implementation of finite difference simulation of the PMF model (S. Padrick *et al.*, unpublished results) to include a reversible equilibrium between IAPP fiber ends and soluble insulin (see Materials and Methods). The mass action equations that are used to describe the PMF model contain considerable degeneracy owing to the large number of parameters. To generate a qualitative assessment of the validity of this process, we implemented a Monte Carlo search of the rate constants in an attempt to find a solution that accommodates the following four separate kinetic measurements: (1) 25 μM IAPP; (2) 25 μM IAPP, 2 μM insulin; (3) 25 μM IAPP, 2 μM seed; (4) 25 μM IAPP, 2 μM insulin, 2 μM seed (Figure 7). Indeed, a single set of rate constants was found that describes simultaneously all four sets of experimental data.

The resultant simulated rates of fiber formation are all physically plausible (see Materials and Methods). For example, IAPP reactions conducted above the critical concentration are expected to be independent of concentration as a result of the dispersed/aqueous phase equilibrium (Figure 6(a)). In our previous studies, we determined that IAPP fiber formation was independent of concentration over the concentration range of 5–50 μM.[14] Using the association/dissociation rate constants for the dispersed/soluble phase transition obtained from our analysis, we estimate the critical concentration

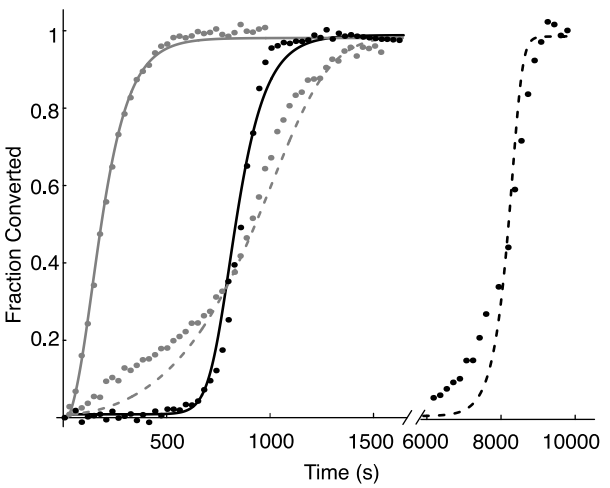

Figure 7. Experimental and simulated data of IAPP fiber formation. Four separate experiments (shown as points) were included and would typically have been fit to a total of 24 parameters to yield four t_{50} values (e.g. see Figure 1(b)). Simulations using only seven rate constants obtained from a Monte Carlo search (see Materials and Methods) are shown as lines and give good agreement with the experimental data. Simulations were generated using initial parameters corresponding to experimental substrate concentrations: 25 μM IAPP (continuous black line), 25 μM IAPP with 2 μM insulin (broken black line), 25 μM IAPP with 2 μM seed (continuous gray line), and 25 μM IAPP with 2 μM insulin and 2 μM seed (broken gray line).

for IAPP fiber formation to be 1.8 μM. In addition, the simulated 25 μM IAPP fiber formation simulation yields an average fiber size of 1400 IAPP monomers/fiber. This is computed by dividing the molar concentration (in monomer units) of fiber by the total number of ends. In studies using electron microscopy, it has been reported that there are 5.2 IAPP molecules/nm for fibers with widths similar to what we observe here.[25] If we combine this density with our observation of fiber lengths of 200–400 nm (Figure 4), then we can estimate we are observing 1560 molecules IAPP/fiber. Clearly, the critical concentration and average fiber lengths estimated from our model are in qualitative agreement with experimental measurement. Therefore, interpretation of our experimental data in the context of the PMF model indicates that insulin inhibits fiber formation predominantly by affecting elongation.

Inhibition of fiber elongation by insulin binding to fiber ends contrasts the near-complete binding of insulin to an IAPP fiber solution as measured by mass spectrometry (Figure 4). If insulin is binding to the ends of fibers, we would like to determine the number of sites available for binding. The *in vitro* produced IAPP fibers we observe by electron microscopy are minimally 200 nm in length. Thus, an upper estimate of the number of ends in a 25 μM solution of IAPP fibers is

$$\frac{(25\ \mu\text{M IAPP molecules} \times 2\ \text{ends/fiber})}{(200\ \text{nm} \times 5.2\ \text{IAPP molecules/nm fiber})}$$

$$= 48\ \text{nM ends}$$

We have shown that addition of 2 μM insulin to a solution of 25 μM IAPP fibers results in virtually all of the insulin associating with the IAPP fibers. If insulin associates with only the fiber ends, this would result in a binding stoichiometry of ~40 insulin molecules/fiber end. This seems unlikely, given a fiber diameter of 10 nm. Instead, we hypothesize that there exists weak, but non-specific binding of insulin to the sides of fibers. Such interactions might be seen to inhibit higher-order aggregation of fibers. Indeed, electron micrographs of IAPP fibers in the presence of insulin show no matting into higher-order arrays (Figure 4(c) and (d)). It is possible for the reduction of higher-order aggregation and inhibition of elongation to be related if non-specific association of insulin with fiber sides can somehow provide a high local concentration of insulin at the fiber ends.

The studies reported here were performed in the presence of substoichiometric concentrations of insulin. Under our conditions, insulin at ratios between 1:100 and 1:5 insulin:IAPP showed a strong kinetic inhibitory effect. In the secretory granule, the insulin:IAPP ratio is closer to 50:1.[16] Extrapolation of our dose-dependent inhibition of fibrillogenesis (Figure 1) to relevant insulin granule concentrations corresponds to a timescale for reaction of several months. However, the lifetime of a secretory granule is on the order of hours.[15] This makes initiation of IAPP fibrillogenesis in the granule unlikely. It has been suggested that decreased ratios of insulin to IAPP may be important in amyloid formation in those afflicted with type II diabetes.[27,28] However, the *in vivo* ratio of insulin:IAPP remains large even when reported variability in expression levels is taken into account. It therefore seems improbable that these perturbations in insulin:IAPP ratios are causal to IAPP fibrillogenesis. Instead, it is likely that an additional process occurs in type II diabetics. Such a process must either act to sharply accelerate IAPP fiber formation, or alternatively, provide an environment that sequesters IAPP from the effects of insulin. A wider understanding of the *in vivo* environment of IAPP nucleation is imperative to our understanding of this disease.

Materials and Methods

Materials

HFIP was obtained from Sigma-Aldrich (Milwaukee, WI) and repurified by fractional distillation. Buffers and salts were obtained from American Bioanalytical (Natick, MA) and J. T. Baker (Phillipsburg, NJ). Synthetic rat IAPP was obtained from Bachem (King of Prussia, PA). Bovine insulin was obtained from Sigma-Aldrich (Milwaukee, WI). Human insulin was obtained from Boehringer Mannheim (Mannheim, Germany). Stock solutions of human and bovine insulin were prepared by solubilizing lyophilized peptide in water, increasing the pH to ~7.0 with sodium hydroxide followed by dilution to final stock concentration of 500 μM in 50 mM Tris–HCl (pH 7.4), 100 mM NaCl. The concentration of insulin was determined using an extinction coefficient of 6000 $M^{-1}\,cm^{-1}$ at 280 nm. The concentration of bovine insulin was determined relative to human insulin using mass spectrometry.[26] Human IAPP was synthesized by standard *t*-Boc synthesis methods and purified in-house. Seed-free stock solutions of IAPP were prepared as described.[22] Briefly, purified lyophilized peptide was solubilized in 7 M guanidine–HCl, and loaded onto a C18 reversed-phase spin column (Amica). The column was washed first with 10% (v/v) acetonitrile and 0.2% (v/v) formic acid, followed by a water wash, followed by elution with 100% HFIP. Stocks of IAPP were stored at ~1 mM in HFIP, which is stable at 4 °C for weeks. The concentration of the hIAPP stock was determined using an extinction coefficient of 2000 $M^{-1}\,cm^{-1}$ at 280 nm calculated from the biopolymer calculator†. This value is consistent with the extinction coefficient calculated from amino acid analysis. The concentration of the rat IAPP stock was determined by comparison to its human counterpart using mass spectrometry.[26]

Fiber formation is initiated upon dilution of IAPP to a final concentration of 25 μM in 50 mM Tris–HCl (pH 7.4), 100 mM NaCl, ± insulin. Since HFIP has a strong effect on IAPP amyloid formation rate, the final concentration of HFIP in the sample is always adjusted to 2.5%

† http://paris.chem.yale.edu/extinct.html

(v/v). Fiber used for seed was produced by dilution of IAPP stock to 25 μM in reaction buffer at 2.5% HFIP. The solution was incubated for 45 minutes at room temperature. Seed age was kept at less than eight hours to ensure reproducibility. All kinetic measurements were performed in triplicate.

Fluorescence

Fluorescence experiments were performed on a PTI QuantaMaster C-61 two-channel fluorescence spectrophotometer fitted with a temperature-controlled cell-holder and automated excitation shutter. Glan-Thompson style plane polarizers and G-factor corrections were used to measure anisotropy. Excitation was accomplished with a 5 nm slit-width centered at 278 nm and detection by a 5 nm slit-width centered at 303 nm. The 200 μl reactions were transferred into a 3 mm × 3 mm cuvette (Helma) and placed into a cell-holder. Dead-times were 30–60 seconds. Anisotropy measurements are displayed in relative units so that reactions conducted at different concentrations of insulin may be compared directly. All measured anisotropies of IAPP/insulin mixtures are consistent with free insulin contributing three times its mole fraction to the apparent total. The factor of 3 reflects the three tyrosine residues contained in insulin.

Mass spectrometry

To test for soluble insulin, 25 μM IAPP reactions containing 2 μM insulin were spun at 18,000*g* in a Beckman bench-top microfuge. The supernatant was removed and analyzed by mass spectrometry[26] after addition of bovine insulin standard to a final concentration of 1 μM. Solutions were prepared for mass spectrometry analysis using the Millipore ZipTip™ system to remove salts, and eluting into 50% acetonitrile, 0.2% formic acid. To test for unreacted IAPP, 25 μM IAPP reactions alone or containing 2 μM insulin were centrifuged at 18,000*g*. An rIAPP standard was added directly to the supernatant. Solutions were prepared for mass spectrometry analysis using Millipore ZipTips™, as above.

Mass spectra were acquired from 200 to 5000 m/z with signal averaging for one minute using a Micromass LCT electrospray time-of-flight mass spectrometer. Atmospheric pressure ionization was performed using borosilicate glass capillaries drawn and sputter-coated in-house. All mass determinations were made using a minimum of three charge states. External calibrations were performed with 20 mM CsI in water ionized under matched instrument conditions. The temperature of the mass spectrometer ionization source was maintained at 20–25 °C.

Electron microscopy

For the images and analysis reported here, the following samples were prepared (see above) twice on separate occasions: 25 μM IAPP, 25 μM IAPP with 2 μM insulin, and 25 μM IAPP with 5 μM insulin. Reactions were incubated for 12 hours. Three microliters of each fiber solution was placed on prepared grids and incubated for one minute. Carbon-coated copper grids were prepared in-house and glow-discharged at 30 mA for 30 seconds prior to application of sample. Grids were stained with 3 μl of 1% (w/v) phosphotungstic acid for one minute. Images were taken using a Philips Technai 12 operating at 120 kV accelerating voltages. Images were collected using a 1000 × 1000 pixel Gatan 794 slow-scan CCD at a magnification of 15,000X and 8 μm underfocus.

Analysis

Simulated kinetic profiles were generated using finite difference methods in Mathematica (Wolfram Research, Inc., Champaign, IL) (S. Padrick *et al.*, unpublished results). The following rate laws were used:

$$\frac{dDP}{dt} = k_{aDP}(M[t])(DP[t]) - k_{dDP}(DP[t]) \quad (1)$$

$$\frac{dM}{dt} = -k_{aDP}(M[t])(DP[t]) + k_{dDP}(DP[t]) - nk_{nuc1}(M[t])^n - k_{elong}(M[t])(Ends[t]) - k_{nuc2}(M[t])(Fiber[t]) \quad (2)$$

$$\frac{dEnds}{dt} = k_{nuc1}(M[t])^n + k_{nuc2}(M[t])(Fiber[t]) - k_{aI}(Ends[t])(I[t]) + k_{dI}(IEnds[t]) \quad (3)$$

$$\frac{dFiber}{dt} = nk_{nuc1}(M[t])^n + k_{nuc2}(M[t])(Fiber[t]) + k_{elong}(M[t])(Ends[t]) \quad (4)$$

$$\frac{dI}{dt} = -k_{aI}(Ends[t])(I[t]) + k_{dI}(IEnds[t]) \quad (5)$$

$$\frac{dIEnds}{dt} = k_{aI}(Ends[t])(I[t]) - k_{dI}(IEnds[t]) \quad (6)$$

Where DP = IAPP in the dispersed phase; M = IAPP in the aqueous phase; *Fiber* = IAPP in the fiber state (in monomer units); *Ends* = fiber ends (elongation competent); I = insulin; *IEnds* = fiber ends bound by insulin (elongation incompetent); n = nucleus size.

Rate constants: k_{aDP} = incorporation of M into DP; k_{dDP} = dissociation of M from DP; k_{nuc1} = formation of *Ends* by primary nucleation; k_{nuc2} = formation of *Ends* by secondary nucleation; k_{elong} = elongation of *Fibers* with M; k_{aI} = association of I to *Ends*; k_{dI} = dissociation of I and *Ends* from *IEnds*.

Boundary conditions (i.e. concentrations at $t = 0$) were chosen to match experimental conditions. The initial concentration of ends used in the seeded simulations was derived from the concentration of Fiber and Ends at $t = 1200$ seconds in the 25 μM IAPP simulation. This was designed to reflect the experimental seeding conditions. Nucleus size, n, was arbitrarily set to 2. A Monte Carlo, i.e. random, search for one set of rate constants that would accommodate four experimental data sets simultaneously was performed. One solution was obtained with the rates:

$$k_{nuc1} = 3.5 \times 10^{-6}\ \mathrm{M^{-1}\ s^{-1}}$$

$$k_{nuc2} = 8.0\ \mathrm{M^{-1}\ s^{-1}}$$

$$k_{elong} = 1.7 \times 10^{7}\ \mathrm{M^{-1}\ s^{-1}}$$

$$k_{aI} = 5.0 \times 10^{8}\ \mathrm{M^{-1}\ s^{-1}}$$

$$k_{dI} = 19\ \mathrm{s}^{-1}$$

$$k_{aDP} = 5550\ \mathrm{M}^{-1}\ \mathrm{s}^{-1}$$

$$k_{dDP} = .010\ \mathrm{s}^{-1}$$

The simulation shown in Figure 1(c) was obtained by using the above mass action equations and rates, with the exception of k_{nuc2}, which was set to zero to simulate a reaction in the absence of secondary nucleation.

Acknowledgements

We thank J. Knight, J. Williamson, S. Padrick, and J. Su for critical reading of this manuscript. We thank V. Unger, B. Koo, and J. Knight for assistance with electron microscopy. This work was supported by grants from the National Institutes of Health (DK54899) and the Pew charitable trusts (PO219SC). A.D.M. is a Pew scholar in the biomedical sciences. J.L. received support from an NIH training grant (5T32GM07223).

References

1. Kelly, J. W. (1996). Alternative conformations of amyloidogenic proteins govern their behavior. *Curr. Opin. Struct. Biol.* **6**, 11–17.
2. Rochet, J. C. & Lansbury, P. T., Jr (2000). Amyloid fibrillogenesis: themes and variations. *Curr. Opin. Struct. Biol.* **10**, 60–68.
3. Sunde, M. & Blake, C. (1997). The structure of amyloid fibrils by electron microscopy and X-ray diffraction. *Advan. Protein Chem.* **50**, 123–159.
4. Blake, C. & Serpell, L. (1996). Synchrotron X-ray studies suggest that the core of the transthyretin amyloid fibril is a continuous beta-sheet helix. *Structure*, **4**, 989–998.
5. Safar, J., Wille, H., Itri, V., Groth, D., Serban, H., Torchia, M., Cohen, F. E. & Prusiner, S. B. (1998). Eight prion strains have PrP(Sc) molecules with different conformations. *Nature Med.* **4**, 1157–1165.
6. Chien, P. & Weissman, J. S. (2001). Conformational diversity in a yeast prion dictates its seeding specificity. *Nature*, **410**, 223–227.
7. Hoppener, J. W., Ahren, B. & Lips, C. J. (2000). Islet amyloid and type 2 diabetes mellitus. *N. Engl. J. Med.* **343**, 411–419.
8. Jaikaran, E. T. & Clark, A. (2001). Islet amyloid and type 2 diabetes: from molecular misfolding to islet pathophysiology. *Biochim. Biophys. Acta*, **1537**, 179–203.
9. Kapurniotu, A. (2001). Amyloidogenicity and cytotoxicity of islet amyloid polypeptide. *Biopolymers*, **60**, 438–459.
10. Cooper, G. J., Willis, A. C., Clark, A., Turner, R. C., Sim, R. B. & Reid, K. B. (1987). Purification and characterization of a peptide from amyloid-rich pancreases of type 2 diabetic patients. *Proc. Natl Acad. Sci. USA*, **84**, 8628–8632.
11. Westermark, P., Wernstedt, C., Wilander, E., Hayden, D. W., O'Brien, T. D. & Johnson, K. H. (1987). Amyloid fibrils in human insulinoma and islets of Langerhans of the diabetic cat are derived from a neuropeptide-like protein also present in normal islet cells. *Proc. Natl Acad. Sci. USA*, **84**, 3881–3885.
12. Lorenzo, A., Razzaboni, B., Weir, G. C. & Yankner, B. A. (1994). Pancreatic islet cell toxicity of amylin associated with type-2 diabetes mellitus. *Nature*, **368**, 756–760.
13. Janson, J., Ashley, R. H., Harrison, D., McIntyre, S. & Butler, P. C. (1999). The mechanism of islet amyloid polypeptide toxicity is membrane disruption by intermediate-sized toxic amyloid particles. *Diabetes*, **48**, 491–498.
14. Padrick, S. B. & Miranker, A. D. (2002). Islet amyloid: phase partitioning and secondary nucleation are central to the mechanism of fibrillogenesis. *Biochemistry*, **41**, 4694–4703.
15. Hutton, J. C. (1989). The insulin secretory granule. *Diabetologia*, **32**, 271–281.
16. Westermark, P., Li, Z. C., Westermark, G. T., Leckstrom, A. & Steiner, D. F. (1996). Effects of beta cell granule components on human islet amyloid polypeptide fibril formation. *FEBS Letters*, **379**, 203–206.
17. Mosselman, S., Hoppener, J. W., Zandberg, J., van Mansfeld, A. D., Geurts van Kessel, A. H., Lips, C. J. & Jansz, H. S. (1988). Islet amyloid polypeptide: identification and chromosomal localization of the human gene. *FEBS Letters*, **239**, 227–232.
18. Harper, J. D. & Lansbury, P. T., Jr (1997). Models of amyloid seeding in Alzheimer's disease and scrapie: mechanistic truths and physiological consequences of the time-dependent solubility of amyloid proteins. *Annu. Rev. Biochem.* **66**, 385–407.
19. Charge, S. B., de Koning, E. J. & Clark, A. (1995). Effect of pH and insulin on fibrillogenesis of islet amyloid polypeptide *in vitro*. *Biochemistry*, **34**, 14588–14593.
20. Janciauskiene, S., Eriksson, S., Carlemalm, E. & Ahren, B. (1997). B cell granule peptides affect human islet amyloid polypeptide (IAPP) fibril formation *in vitro*. *Biochem. Biophys. Res. Commun.* **236**, 580–585.
21. Kudva, Y. C., Mueske, C., Butler, P. C. & Eberhardt, N. L. (1998). A novel assay in vitro of human islet amyloid polypeptide amyloidogenesis and effects of insulin secretory vesicle peptides on amyloid formation. *Biochem. J.* **331**, 809–813.
22. Padrick, S. B. & Miranker, A. D. (2001). Islet amyloid polypeptide: identification of long-range contacts and local order on the fibrillogenesis pathway. *J. Mol. Biol.* **308**, 783–794.
23. Ferrone, F. (1999). Analysis of protein aggregation kinetics. *Methods Enzymol.* **309**, 256–274.
24. Goldsbury, C., Kistler, J., Aebi, U., Arvinte, T. & Cooper, G. J. (1999). Watching amyloid fibrils grow by time-lapse atomic force microscopy. *J. Mol. Biol.* **285**, 33–39.
25. Goldsbury, C. S., Cooper, G. J., Goldie, K. N., Muller, S. A., Saafi, E. L., Gruijters, W. T. *et al.* (1997). Polymorphic fibrillar assembly of human amylin. *J. Struct. Biol.* **119**, 17–27.
26. Larson, J. L., Ko, E. & Miranker, A. D. (2000). Direct measurement of islet amyloid polypeptide fibrillogenesis by mass spectrometry. *Protein Sci.* **9**, 427–431.
27. Westermark, G. T., Leckstrom, A., Ma, Z. & Westermark, P. (1998). Increased release of IAPP in response to long-term high fat intake in mice. *Horm. Metab. Res.* **30**, 256–258.

28. Mulder, H., Martensson, H., Sundler, F. & Ahren, B. (2000). Differential changes in islet amyloid polypeptide (amylin) and insulin mRNA expression after high-fat diet-induced insulin resistance in C57BL/6J mice. *Metabolism*, **49**, 1518–1522.

Edited by F. E. Cohen

(Received 23 June 2003; received in revised form 6 October 2003; accepted 16 October 2003)